Photofragment angular momentum polarization from dissociation of hydrogen peroxide near 355 nm

Photofragment angular momentum polarization from dissociation of hydrogen peroxide near 355 nm

Andrew J. Alexander

Citation: J. Chem. Phys. **118**, 6234 (2003); doi: 10.1063/1.1557920
View online: http://dx.doi.org/10.1063/1.1557920
View Table of Contents: http://jcp.aip.org/resource/1/JCPSA6/v118/i14
Published by the AIP Publishing LLC.

Photofragment angular momentum polarization from dissociation of hydrogen peroxide near 355 nm

Andrew J. Alexander[a)]
School of Chemistry, University of Edinburgh, West Mains Road, Edinburgh, EH9 3JJ, United Kingdom

(Received 5 December 2002; accepted 15 January 2003)

Hydrogen peroxide (H_2O_2) was photodissociated at around 355 nm, using both linearly and circularly polarized light. OH($^2\Pi$) rotational distributions, spin–orbit branching ratios, lambda doublet populations, and angular momentum $\boldsymbol{J}$ polarization in the laboratory and molecule frames were measured by polarized laser probing of the products using laser induced fluorescence. The effects of dynamical torsion and parent molecule bending vibrations on product rotational alignment is discussed, and evidence supporting preferential dissociation of ground-state molecules far from the equilibrium configuration is presented. Possible mechanisms for orientation of product angular momentum in the molecule frame are discussed, and evidence is presented that interference occurs between OH molecules dissociating via the $\tilde{A}$ and $\tilde{B}$ electronic states of H_2O_2. © *2003 American Institute of Physics.* [DOI: 10.1063/1.1557920]

I. INTRODUCTION

Directional properties of angular momentum, and their correlations with fragment velocities, have played a key role in the study of molecular photodissociation.[1] Currently there is a growing interest in molecules that dissociate via more than one pathway leading to a single product.[2,3] This may happen, for example, as the result of mixed transitions to excited states, or by nonadiabatic transitions that occur during the dissociation. In the limit of diatomic photodissociation, transition moments may be parallel or perpendicular to the bond axis. Often, states exhibiting parallel or perpendicular transitions are overlapped in the dissociation spectrum, and this can have significant effects on the directions of the products and their angular momenta. Most of the primary studies of the photodissociation of small molecules were carried out at the absorption maxima, or at convenient laser wavelengths.[1] However, photodissociation studies at wavelengths far from the absorption maximum allow us to investigate interesting regions that may be rich dynamically, e.g., in the low-energy (long photolysis wavelength) tails of the absorption spectrum, where a weaker transition is becoming competitive with a stronger feature.

At 350 nm, the absorption cross section of H_2O_2 vapor is 4×10^{-22} cm^2, one order of magnitude lower than at 266 nm, and some 3 orders of magnitude smaller than the cross section at 193 nm.[4] The ultraviolet dissociation of H_2O_2 has been studied by a number of groups at different wavelengths: 193,[5,6] 248,[7,8] 266,[6,9–11] and 355 nm.[12] Brouard *et al.*[13] studied dissociation of H_2O_2 at 308, 351, 390, and 455 nm to investigate the long-wavelength near-threshold dynamics. At 193 nm, the angular anisotropy parameter, $\beta=0.0\pm0.02$, suggesting that the dissociation proceeds via a mixture of perpendicular ($\perp$) and parallel ($\parallel$) transitions, and the dissociation is believed to access the $\tilde{A}(^1A)$ ($\perp$; 62%) and $\tilde{B}(^1B)$ ($\parallel$; 38%) states.[5] In its ground $\tilde{X}(^1A)$ state, the H_2O_2 molecule prefers a twisted conformation with the dihedral angle between the OH molecules $\phi_d\approx112°$, see Fig. 1. Reinsch has calculated that the $\tilde{A}$ state transition moment lies along the C_2 axis, and the $\tilde{B}$ state transition moment lies very nearly parallel to the O–O bond axis.[14] Both the $\tilde{A}$ and $\tilde{B}$ states are strongly repulsive, but in terms of the dihedral angle, the $\tilde{A}$ state minimum is a *trans* conformation ($\phi_d=180°$), and the $\tilde{B}$ state minimum is *cis* ($\phi_d=0°$). Such a change in torsional conformation on accessing the excited states is believed to be responsible for the observation of a strong correlation of $\boldsymbol{J}\parallel\boldsymbol{v}$ at 266 nm, where $\boldsymbol{v}$ is the OH velocity.[10] Photodissociation of H_2O_2 becomes almost purely perpendicular at 266 nm ($\beta=-0.71$)[10] and then shows mixing again by 351 nm ($\beta=-0.10$).[13] Brouard *et al.* presented compelling evidence that the long-wavelength ($\lambda>310$ nm) dissociation of H_2O_2 *again* accesses both the $\tilde{A}$ and $\tilde{B}$ states. Energy requirements dictate that the ground-state molecules that are dissociated at longer wavelengths are either thermally excited, or more probably that the Franck–Condon factor selects a subset of molecules far from their equilibrium configurations.[8,13]

In this paper, we report measurements on the dissociation of hydrogen peroxide (H_2O_2) around 355 nm, in the long-wavelength tail of the ultraviolet (UV) absorption spectrum. Measurements of angular momentum polarization give a detailed picture of state-specific dissociation mechanisms for this molecule, showing that dissociation from nonequilibrium configurations of the ground-state parent molecule occurs. Evidence for interference between multiple dissociating electronic states is also reported. The experimental apparatus is briefly described in Sec. II, the polarization parameters are introduced in Sec. III, laboratory frame and molecule frame polarization results are presented in Secs. IV and V, respectively, and a final summary is given in Sec. VI.

[a)]Electronic mail: andrew.alexander@ed.ac.uk

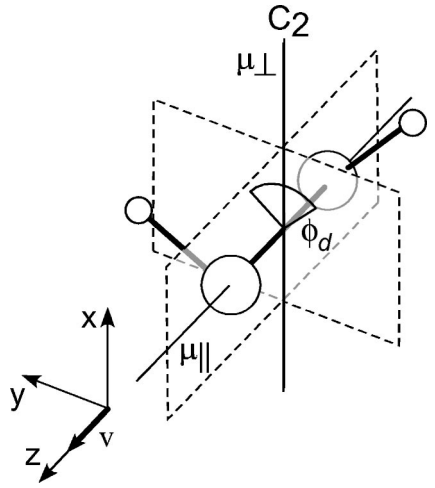

FIG. 1. Schematic diagram showing an H_2O_2 twisted ground-state $\tilde{X}(^1A)$ conformer. The C_2 symmetry axis is shown, along with the directions of the parallel ($\mu_{||}$) and perpendicular ($\mu_{\perp}$) transition moments, as calculated by Reinsch (Ref. 14). The dihedral angle ϕ_d is the angle between the two OH bonds, as shown. The molecule frame used in the present work is also shown, with the z axis defined by the product OH velocity vector $\boldsymbol{v}$, and the x axis lying along the C_2 symmetry axis. Note that the conformer shown is chiral. A racemic mixture of H_2O_2 at 300 K would contain equal amounts of left and right handed conformers.

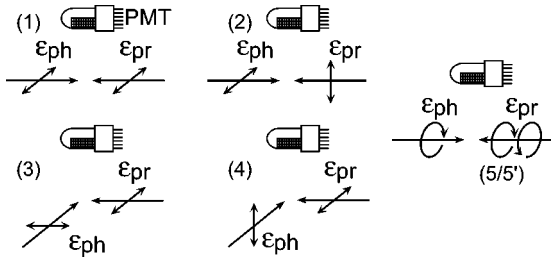

FIG. 2. Schematic diagram showing experimental geometries used in the present study, with the direction of the laser beams shown as straight single-head arrows, and the photolysis $\boldsymbol{\epsilon}_{ph}$ and probe $\boldsymbol{\epsilon}_{pr}$ laser electric field vectors as labeled. Geometries 5 and 5′ have opposite probe circular polarizations, although we did not determine which was left and which was right circularly polarized. The PMT detector lies above the interaction region in all cases.

II. EXPERIMENT

The experimental setup was very similar to those described in detail previously elsewhere,[6,10] and only a brief description will be given here. A 60% w/v aqueous hydrogen peroxide solution was gently distilled under vacuum and stored in a glass bulb. Only polytetrafluoroethene (PTFE) parts, or stainless steel coated with a film of PTFE, were used in the gas handling manifold. The vapor was constantly flowed thorough a stainless steel reaction cell with six orthogonal arms that had been internally coated with carbon paint. Four arms of the cell contained painted baffles, with four broadband UV anti-reflection coated windows, positioned normal with respect to the incoming light. During the experiments, the total pressure in the cell was kept constant below 100 mTorr.

The photolysis radiation at 355 nm was generated using third harmonic generation from a Continuum Surelite III-10 YAG laser operating at 10 Hz. The beam was passed through a 2 mm diameter iris, and loosely focused using a 250 mm focal length lens. The total power before the lens was on the order of 7 mJ cm^{-2} $pulse^{-1}$. Second harmonic light (532 nm) from the same laser was used to pump a Sirah dye laser (GS-R-2400), which was operated with DCM dye at around 615 nm. The fundamental output from the dye laser was doubled to ~308 nm using a KDP crystal. The quality of polarization was measured using a Glan Laser polarizer (Special Optics, USA) and both the resulting 355 nm and the 308 nm laser radiations were found to be highly linearly polarized (>99.5%). The 308 nm probe radiation was switched between vertical and horizontal linear polarization every shot by synchronizing the laser to the stress cycle of a fused-silica photoelastic modulator (Hinds PEM-90D). Circularly polarized light was produced using zero order quartz quarter-wave plates at 308 and 355 nm (Coherent, UK). Various tests for purity of polarization were carried out, including measurement of null difference signals for molecules in rotational states with $J=0.5$ that should show no alignment. For OH molecules J refers to the total angular momentum, and N is total J excluding spin: for $^2\Pi_{3/2}(F_1)$ $J=N+\frac{1}{2}$, and $^2\Pi_{1/2}(F_2)$ $J=N-\frac{1}{2}$.

Laser induced fluorescence (1+1 LIF) from the A–X (0,0) band of OH was collected via a fifth arm of the steel cell using a pair of f/1.5 fused-silica plano convex lenses and an interference filter centered at 307.1 nm (Coherent, UK), and was focused onto a photomultiplier tube (Hamamatsu, R3896). Transitions in the present work are labeled $^{\Delta N}\Delta J_{fF}(N)$ where f and F refer to the spin–orbit state of the OH A and X states, respectively. In the case that $\Delta N=\Delta J$, and $f=F$, only one label is given, e.g., $Q_1(3)$ is shorthand for $^QQ_{11}(N=3)$. The fluorescence was collected without analysis of polarization. A schematic diagram of the experimental geometries employed is shown in Fig. 2. The fluorescence signal was amplified with a home-built fast preamplifier and integrated using a boxcar (SRS 250) with a gate width of 50 ns after the probe laser pulse. A photodiode was used to monitor the probe laser power, and experimental checks were carried out to ensure that no saturation of the laser induced fluorescence (LIF) occurred. Since the photodissociation cross section of H_2O_2 at 355 nm is very small, and almost an order of magnitude lower than that at 308 nm, several tests were made to ensure that photolysis at 308 nm did not affect the measurements. Data were transferred to a computer running Labview (National Instruments) by GPIB via a computer interface (SRS 245), and stored according to the probe polarization.

III. EXTRACTION OF THE POLARIZATION PARAMETERS

The intensity of the LIF signal in the laboratory frame is written following Kummel, Sitz, and Zare (KSZ[15])

$$I=C(\det)n(J)\sum_{k,q,J_f}P_{q^{\pm}}^{(k)}A_{q^{\pm}}^{(k)}, \tag{1}$$

TABLE I. Conversion factors between the polarization parameters of Rakitzis *et al.*,[19] the polarization parameters of Vasyutinskii *et al.*,[2,18] and the dynamical functions of Siebbeles *et al.*[17] The directional interpretations of the $\mathbf{a}_q^{(k)}(p)$ parameters in the molecule frame are also shown. A full summary of the physical meaning and directional properties of $k=1,2$ real spherical tensor moments has been tabulated by Miranda *et al.*[20] Note that the conversion factors given in Refs. 21 and 2 are valid only in the semiclassical limit. The $\mathbf{a}_0^{(1)}(\perp)$ parameter does not exist for photolysis of an achiral molecule by linearly polarized light, and for this we have used β appropriate for circularly polarized photolysis radiation. The following equivalences apply $\mathbf{a}_{1+}^{(1)}=-\sqrt{2}\,\mathrm{Re}[\mathbf{a}_1^{(1)}]$, $\mathbf{a}_{1-}^{(1)}=-\sqrt{2}\,\mathrm{Im}[\mathbf{a}_1^{(1)}]$, $\mathbf{a}_{1+}^{(2)}=-\sqrt{2}\,\mathrm{Re}[\mathbf{a}_1^{(2)}]$, and $\mathbf{a}_{2+}^{(2)}=\sqrt{2}\,\mathrm{Re}[\mathbf{a}_2^{(2)}]$.

Rakitzis (Ref. 19)	Vasyutinskii (Refs. 2 and 18)	Siebbeles (Ref. 17)[a]	When positive	When negative
$\mathbf{a}_0^{(1)}(\perp)$	$\frac{3\alpha_1}{1+\beta}$	$\frac{f_1(1,1)}{f_0(1,1)}$	orientation parallel to z	orientation antiparallel to z
$\mathbf{a}_{1+}^{(1)}(\parallel,\perp)$	$3\gamma_1$	$\frac{6\mathrm{Re}[f_1(1,0)]}{f_0(0,0)+2f_0(1,1)}$	orientation parallel to x	orientation antiparallel to x
$\mathbf{a}_{1-}^{(1)}(\parallel,\perp)$	$3\gamma_1'$	$\frac{6\mathrm{Im}[f_1(1,0)]}{f_0(0,0)+2f_0(1,1)}$	orientation parallel to y	orientation antiparallel to y
$\mathbf{a}_0^{(2)}(\parallel)$	$\frac{5(s_2-2\alpha_2)}{1+\beta}$	$\frac{1}{W(J)}\frac{f_2(0,0)}{f_0(0,0)}$	alignment along z	alignment perpendicular to z
$\mathbf{a}_0^{(2)}(\perp)$	$\frac{10(s_2+\alpha_2)}{2-\beta}$	$\frac{1}{W(J)}\frac{f_2(1,1)}{f_0(1,1)}$	alignment along z	alignment perpendicular to z
$\mathbf{a}_{1+}^{(2)}(\parallel,\perp)$	$5\sqrt{3}\gamma_2$	$\frac{6}{W(J)}\frac{\mathrm{Re}[f_2(1,0)]}{f_0(0,0)+2f_0(1,1)}$	alignment along $x+z$	alignment along $x-z$
$\mathbf{a}_{2+}^{(2)}(\perp)$	$\frac{-5\sqrt{3}\eta_2}{(2-\beta)}$	$-\frac{1}{\sqrt{2}W(J)}\frac{f_2(1,-1)}{f_0(1,1)}$	alignment along x	alignment along y

[a] $W(J)=[J(J+1)/(2J+3)(2J-1)]^{1/2}$.

where $C(\mathrm{det})$ is a function of the particular detection apparatus, assumed to be constant for all of our experiments, and $n(J)$ is the population of the initial rotational state J. The sensitivities to angular momentum polarization, $P_{q\pm}^{(k)}$, were calculated using the method described by KSZ, and included known line-strength factors for OH and effects of hyperfine depolarization.[15,16] The laboratory frame (also known as space-fixed frame) polarization moments $A_{q\pm}^{(k)}$ can be written in terms of molecule frame (also known as body-fixed frame, or velocity frame) polarization parameters. The laboratory frame zero order moment $A_0^{(0)}$ can be written

$$4\pi A_0^{(0)}(\theta,\phi)=1+\beta P_2(\cos\theta). \tag{2}$$

The angular variables $(\theta,\ \phi)$ are defined in the laboratory frame (our laboratory frame is identical to Fig. 1 of Ref. 17, with the photolysis electric field vector along the Z axis). $P_2(x)$ is the second Legendre polynomial. The normalization factor 4π ensures that by integration over all angles $\langle A_0^{(0)}\rangle=1$. The beta parameter (β) takes axial recoil limits $+2$ for a pure parallel transition, and -1 for a pure perpendicular transition. In the case of photolysis using circularly polarized light, these limits change to -1 and $+\frac{1}{2}$, respectively.

For photolysis with circular polarization, the laboratory frame orientation moment $A_0^{(1)}$ can be written

$$4\pi A_0^{(1)}(\theta,\phi)=(1+\beta)\mathbf{a}_0^{(1)}(\perp)\cos^2\theta+\tfrac{1}{2}\mathbf{a}_{1+}^{(1)}(\parallel,\perp)\sin^2\theta. \tag{3}$$

For photolysis with linearly polarized light, the $A_0^{(2)}$ and $A_{2+}^{(2)}$ laboratory frame alignment moments can be written

$$\begin{aligned}4\pi A_0^{(2)}(\theta,\phi)=P_2(\cos\theta)\Big[&(1+\beta)\mathbf{a}_0^{(2)}(\parallel)\cos^2\theta\\&+\frac{1}{2}(2-\beta)\mathbf{a}_0^{(2)}(\perp)\sin^2\theta\Big]\\&+\frac{\sqrt{3}}{4}\sin^2\theta[(2-\beta)\mathbf{a}_{2+}^{(2)}(\perp)\sin^2\theta]\\&-\frac{\sqrt{3}}{4}\mathbf{a}_{1+}^{(2)}(\parallel,\perp)\sin^2 2\theta,\end{aligned} \tag{4}$$

$$\begin{aligned}4\pi A_{2+}^{(2)}(\theta,\phi)=\frac{\sqrt{3}}{2}\sin^2\theta\cos 2\phi\Big[&(1+\beta)\mathbf{a}_0^{(2)}(\parallel)\cos^2\theta\\&+\frac{1}{2}(2-\beta)\mathbf{a}_0^{(2)}(\perp)\sin^2\theta\Big]+\frac{1}{4}(1+\cos^2\theta)\\&\times\cos 2\phi[(2-\beta)\mathbf{a}_{2+}^{(2)}(\perp)\sin^2\theta]\\&-\frac{1}{4}\mathbf{a}_{1+}^{(2)}(\parallel,\perp)\sin^2 2\theta\cos 2\phi.\end{aligned} \tag{5}$$

The above equations have been obtained by rotating molecule frame parameters $\mathbf{a}_q^{(k)}(p)$ to the laboratory frame using a transformation similar to Eq. (16) of Bracker *et al.*[18] We have used the molecule frame notation $\mathbf{a}_q^{(k)}(p)$ of Rakitzis *et al.*[19] to distinguish between parameters that originate from parallel $(\parallel)$ and perpendicular $(\perp)$ transitions, and the Hertel–Stoll definitions of real spherical tensor moments have been used (see Table I). We have neglected higher order moments $A_{q\pm}^{(k)}$ with $k>2$. This is partly justifiable because the sensitivities for these moments were found to be small for the transitions and geometries used in the present study.

An average estimate of the effect of not including moments $k>2$ was found to be $<5\%$: Much less than experimental uncertainties in the moments $k\leqslant 2$. Some parameters vanish simply as a result of the symmetry of the H_2O_2 system, see Fig. 1. The racemic mixture of H_2O_2 equates to the existence of three orthogonal reflection planes, with two that include the C_2 axis: This causes all $\mathbf{a}_{q-}^{(k)}(p)$, $\mathbf{a}_{1+}^{(2)}(\|)$ and $\mathbf{a}_{1+}^{(2)}(\perp)$ to vanish (see Fig. 1). The $\mathbf{a}_{2+}^{(2)}(\|)$ vanishes, because the $\tilde{B}$-state transition moment lies parallel to the O–O bond axis,[14] and the H atom angular positions are not correlated with it. The resulting equations show that the H_2O_2 molecule behaves much like a diatomic molecule, and that the perpendicular transition moment $\boldsymbol{\mu}(\perp)$ and the velocity $\boldsymbol{v}$ define a specific plane in the molecule frame.

The interpretation of molecule frame parameters $\mathbf{a}_q^{(k)}(\|,\perp)$ that arise due to coherence between parallel and perpendicular transitions is not straightforward in the case of polyatomic parent species. The electronic transition moment may not be exactly parallel or perpendicular to the asymptotic direction of the lysing bond, and the coherent moments can be observed from incoherent transitions of either symmetry. For example, if a linear triatomic happens to be excited during bending vibration, an observed $\mathbf{a}_q^{(k)}(\|,\perp)$ may originate from parallel and perpendicular *projections* of an in-plane transition moment, as discussed by Ahmed *et al.*[22] for NO_2 dissociation, and by Kim *et al.*[23] in the case of OCS dissociation. Likewise, the $\mathbf{a}_{2+}^{(2)}(\perp)$ parameter for a polyatomic molecule may result from parent bending, rather than coherence between excited $|\Omega|=1$ states of the parent molecule. In the present report, we keep the $(\|,\perp)$ notation, and will develop our interpretation with the above caveat in mind. The Rakitzis alignment parameters are easily converted to the α_K parameters of Vasyutinskii and co-workers,[2,18] or the dynamical parameters $f_K(q,q')$ of Siebbeles *et al.*,[17] and for convenience these conversions are summarized in Table I. Equations relating α_K to the bipolar moments of Dixon[24] have appeared elsewhere.[21,25] Monte Carlo simulations of Doppler line shapes $D(\nu)$ were obtained by projecting the total distribution [Eq. (1)] onto the Doppler axis, and integrating contributions that shared the same projection on this axis. The extraction of the polarization moments are greatly complicated by the two photons of the (1+1) LIF that propagate in different directions. Of course it would be possible to rewrite the $A_{q\pm}^{(k)}$ laboratory frame equations in the Doppler frame, however, this would produce very cumbersome general expressions. Experimental Doppler line shapes were fitted, by nonlinear least-squares methods, using a basis set of simulated line shapes with known values of the molecule frame parameters, as described in detail elsewhere.[19,26]

IV. LABORATORY FRAME RESULTS

A. Rotational distributions

Rotational distributions of the OH molecule were obtained by scanning over the Q_1, Q_2, R_1, and R_2 branches of the LIF spectrum. Spectra were obtained by timing the PEM to produce light linearly polarized parallel $I_1(\nu)$ or perpendicular $I_2(\nu)$ with respect to the horizontally polarized photolysis light, corresponding to geometries 1 and 2 shown in Fig. 2. In this way it was also possible to obtain the integrated lab frame alignment $\langle A_0^{(2)}\rangle$ as a function of rotation (see Sec. IV B below). Sum and difference spectra were formed by taking $I_{\rm iso}^{1,2}(\nu)=I_1(\nu)+\frac{5}{2}I_2(\nu)$ and $I_{\rm aniso}^{1,2}(\nu)=I_1(\nu)-I_2(\nu)$. $I_{\rm iso}^{1,2}(\nu)$ and $I_{\rm aniso}^{1,2}(\nu)$ isolate population and alignment contributions, respectively, and were fitted simultaneously using line strengths and alignment sensitivity factors.[15,16] Note that the factor of 5/2 in the above expression for $I_{\rm iso}^{1,2}(\nu)$ is J dependent, and is obtained from the ratio $-P_0^{(2)}(\text{geometry1})/P_0^{(2)}(\text{geometry 2})$: We have used 5/2 as an approximate mean of this ratio over the Q branch. The raw data are shown in Figs. 3 and 8, and the resulting rotational distributions are shown in Fig. 4. The peak in the rotational distribution around $N=3$ agrees with previous work by Crim and co-workers.[27] We calculate the average fraction of available energy going into rotation is $\langle f_{\rm rot}\rangle=4.5\%$, with $\langle E_{\rm rot}\rangle=508\ \text{cm}^{-1}$, in good agreement with Brouard *et al.*[13] Although it is not expected that the rotational distribution should follow a Boltzmann distribution,

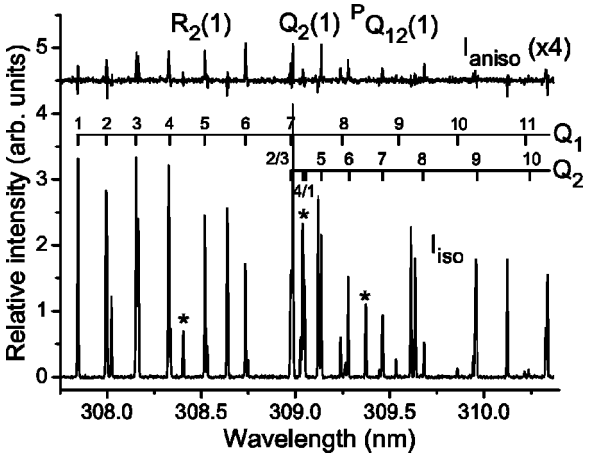

FIG. 3. Isotropic $I_{\rm iso}^{1,2}(\nu)$ and anisotropic $I_{\rm aniso}^{1,2}(\nu)$ LIF composite spectra, scanned over the Q_1 and Q_2 branches. The data were taken using linear polarizations (geometries 1 and 2 in Fig. 2). The anisotropic spectrum has been magnified ($\times 4$) and vertically displaced for clarity. Some of the $J=0.5$ lines that cannot be aligned (and should therefore have no anisotropic signal) have been identified with asterisks.

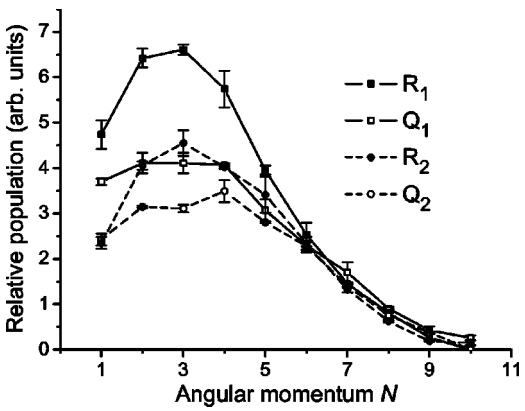

FIG. 4. Rotational distributions as function of the rotational quantum number N, obtained from the isotropic spectra shown in Figs. 3 and 8.

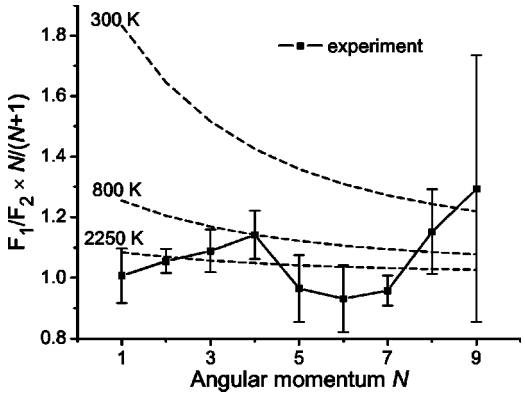

FIG. 5. Ratios of spin–orbit state populations as a function of the rotational quantum number, N. The ratio of populations has been scaled by the factor $N/(N+1)$ to account for rotational J degeneracies in the two OH spin–orbit states $\Pi_{3/2}(F_1)$ and $\Pi_{1/2}(F_2)$. The dashed lines are theoretical distributions at different temperatures, obtained using a Boltzmann distribution.

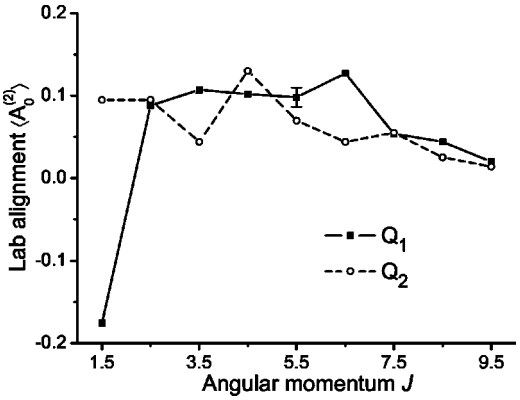

FIG. 7. Integrated laboratory frame alignment moment $A_0^{(2)}$ for each of the OH spin–orbit states as a function of the total angular momentum quantum number, J. These moments were obtained by fitting the anisotropic rotational spectrum shown in Fig. 3; see text for details.

nevertheless the data can be approximated by the rotational temperatures $T=650\pm16$ K for the F_1 states and $T=650\pm32$ K for the F_2 states.

Spin–orbit branching ratios as a function of N are shown in Fig. 5, along with the Boltzmann distributions expected at various temperatures. The experimental ratios are all close to unity, implying that there is no preference for production of either spin–orbit state, in agreement with results at other wavelengths.[13]

Lambda-doublet ratios for the A″/A′ Π states are shown in Fig. 6. There appears to be a slight preference for the A′ Λ-doublet at low J, moving towards more A″ population at high J. In the limit of high J, we can associate the A″ lambda doublet with molecules in which the unpaired electron populates a p-orbital that is perpendicular to the plane of rotation.[28] Gericke *et al.* have determined the expected orbital populations resulting from excitation to the $\tilde{A}(^1A)$, $\tilde{B}(^1B)$, and $\tilde{C}(^1A)$ states using a simple molecular-orbital picture.[10] They concluded that there should be no strong preference for population of either Λ-doublet, except for dissociation via the $\tilde{C}$ state. The $\tilde{C}$ state seems an unlikely candidate for the dissociation at 355 nm, because it lies much higher in energy than the $\tilde{A}$ or $\tilde{B}$ states. Morita and Kato have reported calculations that suggest that crossing from $\tilde{A}$ to ^3B, as a result of spin–orbit coupling, causes preferential population of the A'' state.[29] Our Λ-doublet ratios are very similar to the 193 nm photolysis results of Gericke *et al.*, consistent with the hypothesis of Brouard *et al.* that the $\tilde{A}$ and $\tilde{B}$ states are the main states involved at 355 nm.[13]

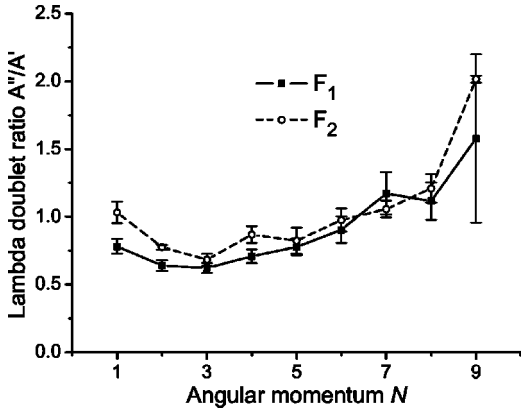

FIG. 6. Ratios of lambda doublet populations $\Pi(A'')/\Pi(A')$ as a function of the rotational quantum number, N, for each of the OH spin–orbit states.

B. Laboratory frame alignment

The laboratory frame alignment integrated over all translational directions of the product, $\langle A_0^{(2)} \rangle$, is plotted as a function of J in Fig. 7. Since the Q branches have the highest sensitivity to the $A_0^{(2)}$, only Q branch data were analyzed. Rotational transitions that should show zero alignment (because $J=0.5$) are highlighted in Fig. 3. Integrating Eq. (4) over all angles θ, ϕ, we obtain

$$\langle A_0^{(2)} \rangle = \frac{2}{15}\left[(1+\beta)\mathbf{a}_0^{(2)}(\|) - \frac{1}{2}(2-\beta)\mathbf{a}_0^{(2)}(\perp)\right] + \frac{2}{5\sqrt{3}}[-\mathbf{a}_{1+}^{(2)}(\|,\perp) + (2-\beta)\mathbf{a}_{2+}^{(2)}(\perp)], \quad (6)$$

that is, $\langle A_0^{(2)} \rangle = -2(\alpha_2+\gamma_2+\eta_2)$ in the lab-frame notation of Vasyutinskii *et al.*[18] The classical limits of alignment in the laboratory are -1 to $+2$. It is clear that the experimental results are small compared to their limiting values, and actually appear to decrease slightly with increasing J. Following the classical arguments of Docker *et al.*,[7] we note that $\langle A_0^{(2)} \rangle = 2\beta\langle P_2(\boldsymbol{J}\cdot\boldsymbol{v})\rangle/5$. Given that $\beta<0$, we might expect to find that the positive $\langle A_0^{(2)} \rangle$ that we measure in the laboratory frame results from a correlation of $\boldsymbol{J}\perp\boldsymbol{v}$ in the molecule frame, i.e., $\mathbf{a}_0^{(2)}(p)<0$. Such a conclusion would be erroneous, and arises because $\boldsymbol{J}$ is not axially symmetric around $\boldsymbol{v}$ when the parameters $\mathbf{a}_{1+}^{(2)}(\|,\perp)$ and $\mathbf{a}_{2+}^{(2)}(\perp)$ are nonzero, as we shall show in more detail in Sec. V A below.

An interesting feature of Fig. 3 is the alignment observed for the $Q_1(1)$ line. $\langle A_0^{(2)} \rangle = -0.18$ for F_1 ($J=1.5$) has twice the magnitude and has opposite sign to $\langle A_0^{(2)} \rangle = +0.095$ for the F_2 ($J=1.5$) state. It is possible that this stems from an increased contribution from the coherent $\mathbf{a}_{1+}^{(2)}(\|,\perp)$ parameter to the overall alignment in Eq. (6). The low $J=1.5$ states

differ significantly in the composition of the total angular momentum, made up from electronic and rotational angular momentum. In Hund's case (a), for F_1 ($J=1.5$), the total J is purely electronic, being composed of spin and orbital angular momentum to give a total projection $\Omega=1.5$ on the bond axis: The molecule has no nuclear rotation. In contrast, F_2 ($J=1.5$) is made up of spin + orbital angular momentum $\Omega=0.5$ with a further unit of rotational angular momentum, giving total $J=1.5$. Therefore, the exceptional alignment of OH F_1 ($J=1.5$) molecules could result from pure electronic alignment created by the absorption of the photolysis photon, whereas all of the other J states have an additional alignment contribution from the rotation of the OH molecule. The rotational alignment is dependent on the shape of the ground-state potential energy surface, including contributions from the torsional and bending motions of the parent H_2O_2 molecule. The rotational alignment of the OH also depends on the shape of the excited state potential energy surface, *viz.*, the change in torsional minimum from $\phi_d=112°$ in the $\tilde{X}$ state to $\phi_d=180°$ and $0°$ on accessing the $\tilde{A}$ or $\tilde{B}$ states, respectively.

C. Laboratory frame orientation

Laboratory frame orientation measurements were carried out using counter-propagating photolysis and probe beams, both of which were circularly polarized—see geometries 5 and 5′ in Fig. 2. Using these geometries, it is possible to determine the laboratory frame orientation, integrated over all product directions,

$$\langle A_0^{(1)}\rangle=\tfrac{1}{3}[(1+\beta)\mathbf{a}_0^{(1)}(\|)+\mathbf{a}_{1+}^{(1)}(\|,\perp)], \tag{7}$$

that is $\langle A_0^{(1)}\rangle=\alpha_1+\gamma_1$ using the lab-frame notation of Vasyutinskii *et al.*[2] Transitions with $\Delta J=\pm 1$ have the highest sensitivity to orientation, and therefore spectra of the R_1 and R_2 branches were taken. Sum and difference spectra were calculated as $I_{\rm iso}^{5,5'}(\nu)=I_5(\nu)+I_{5'}(\nu)$ and $I_{\rm aniso}^{5,5'}(\nu)=I_5(\nu)-I_{5'}(\nu)$, although we were unable to determine the absolute handedness of circularly polarized light: We only know that geometries 5 and 5′ have opposite circular probe polarizations. The spectra are shown in Fig. 8. The "isotropic" spectrum $I_{\rm iso}^{5,5'}(\nu)$ retains a residual contribution from lab frame alignment $A_0^{(2)}$. However, the R branch sensitivities to alignment in geometry 5 are very small, e.g., $P_0^{(2)}=0.249$ for $R_1(5)$ compared with $P_0^{(1)}=1.421$. Lower sensitivity to alignment, combined with the very low integrated $\langle A_0^{(2)}\rangle$ as determined above, mean that effects of alignment on the measured $\langle A_0^{(1)}\rangle$ are minimized. Also, there are no higher *integrated* $\langle A_q^{(k)}\rangle$ moments in the laboratory frame.[17]

Since we were unable to determine the absolute handedness of our circularly polarized light, the sign of $\langle A_0^{(1)}\rangle$ cannot be determined. The magnitude of laboratory frame orientation $|\langle A_0^{(1)}\rangle|$, is plotted as a function of J in Fig. 9. Results derived from $R_1(1)$ were unreliable due to blending of lines in the spectrum, and so the value derived from the $P_1(1)$ transition has been plotted instead. The values from $P_1(2)$ and $R_2(2)$ show good agreement within uncertainties. The maximal $\mathbf{a}_0^{(1)}(\perp)=\sqrt{J/J+1}$. Assuming the coherent $\mathbf{a}_{1+}^{(1)}(\|,\perp)=0$, and $\beta=0.1$, we estimate from Eq. (7) that the maximal $|\langle A_0^{(1)}\rangle|$ would be 0.212 at $J=0.5$, rising to 0.349 at $J=9.5$. Clearly, the observed $|\langle A_0^{(1)}\rangle|$ lie well below these limits. The $|\langle A_0^{(1)}\rangle|$ appears to peak at around $J=4.5$ (F_1) and $J=6.5$ (F_2), showing decreased orientation at lower and higher J. Since the racemic H_2O_2 mixture is achiral, the $|\langle A_0^{(1)}\rangle|$ in the laboratory frame results from the *helicity* of the circularly polarized photolysis photon, so that helicity of the system is conserved in the laboratory frame. On the other hand, the circularly polarized photon acts upon the electrons in parent molecule, i.e., the photon has no selectivity over the helicity of motion of the nuclei. Although $|\langle A_0^{(1)}\rangle|$ for $J=0.5$ (F_2) is slightly higher than that for $J=1.5$ (F_2), there is no variation in $|\langle A_0^{(1)}\rangle|$ at low J as dramatic as was observed for the $\langle A_0^{(2)}\rangle$. This is consistent with the orientation being produced only as electronic orientation over the entire range of J, in comparison to the electronic and rotational alignment mechanisms discussed in Sec. IV B. The lower $|\langle A_0^{(1)}\rangle|$ at low J may be due to increasing influence from the coherent $\mathbf{a}_{1+}^{(1)}(\|,\perp)$, as we shall discuss in Sec. V B.

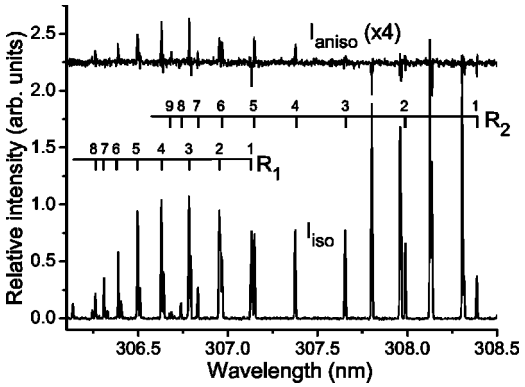

FIG. 8. Isotropic $I_{\rm iso}^{5,5'}(\nu)$ and anisotropic $I_{\rm aniso}^{5,5'}(\nu)$ LIF composite spectra, scanned over the R_1 and R_2 branches. The data were taken using circular polarizations (geometries 5 and 5′ in Fig. 2) The anisotropic spectrum has been magnified and vertically displaced for clarity.

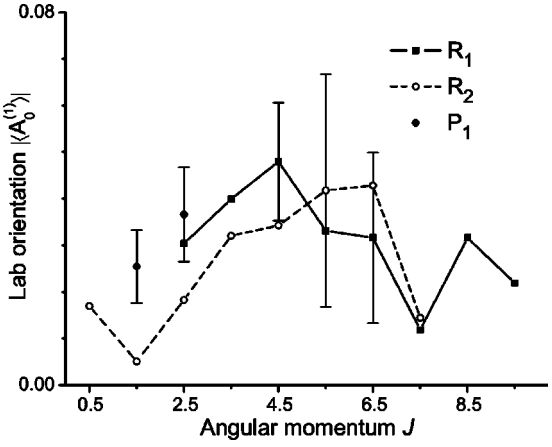

FIG. 9. Integrated laboratory frame orientation moment $|\langle A_0^{(1)}\rangle|$ for each of the spin–orbit states as a function of the total angular momentum quantum number, J. These moments were obtained by fitting the anisotropic rotational spectrum shown in Fig. 3; see text for details. Error bars represent single standard deviations from multiple measurements.

TABLE II. Beta parameters determined from Doppler line shapes for selected lines; see text for details.

Transition	Angular momentum J	Beta parameter β
${}^{P}Q_{12}(1)$	0.5	-0.13 ± 0.05
$R_2(1)$	0.5	-0.10 ± 0.07 (Ref.13)
$P_1(5)$	5.5	-0.21 ± 0.04
$P_2(5)$	4.5	-0.18 ± 0.05
$P_2(8)$	7.5	-0.04 ± 0.05

V. DOPPLER MEASUREMENTS

In Sec. III, the laboratory polarization moments $A_q^{(k)}$ were given in terms of molecule frame polarization parameters $\mathbf{a}_{q\pm}^{(k)}(p)$. The molecule frame parameters can be obtained from measurements using different geometries and transitions in the laboratory frame, and by resolving product velocity. The directional part of the product velocity becomes especially important in the case of dissociations involving transitions of mixed $(\|,\perp)$ symmetry since the fragments travel in different directions, even if they have similar speeds.

A. Alignment

Fitting of Doppler line shapes to obtain polarization parameters requires the translational anisotropy parameter β. The β parameter was determined by making measurements using geometries 3 and 4 for the ${}^{P}Q_{12}(1)$, $P_1(5)$, $P_2(5)$, and $P_2(8)$ transitions. The photolysis electric field vector was parallel (geometry 3) or perpendicular (geometry 4) to the Doppler axis (the probe laser propagation direction), see Fig. 2. Approximately isotropic and anisotropic composite Doppler line shapes were formed $D_{\rm iso}^{3,4}(\nu)=D_3(\nu)+2D_4(\nu)$, $D_{\rm aniso}^{3,4}(\nu)=D_3(\nu)-D_4(\nu)$. These composite line shapes are not ideal, because they include residual contributions from the alignment $A_q^{(2)}$. Since the integrated alignment moments $\langle A_0^{(2)}\rangle$ determined in Sec. IV B are relatively small, the approximation holds quite reasonably. Furthermore, the ${}^{P}Q_{12}(1)$ transition originates from $J=0.5$, and cannot exhibit alignment. The experimental composite line shapes were fitted using a basis set of simulated line shapes that include only the zeroth-order moment $A_0^{(0)}(\theta,\phi)$. The results are shown in Table II. The β obtained are in excellent agreement with the results of Brouard *et al.*[13] Using $\beta=-0.13$ for ${}^{P}Q_{12}(1)$, we estimate that the fraction of products produced by perpendicular transition to be 71%.

To determine molecule frame alignment parameters, we made repeated Doppler line shape measurements for the $P_1(5)$ line using geometries 1 to 4. Composite line shapes were formed for pairs of geometries (1,2): $D_{\rm iso}^{1,2}(\nu)=D_1(\nu)+2D_2(\nu)$, $D_{\rm aniso}^{1,2}(\nu)=D_1(\nu)-D_2(\nu)$, and (3,4): $D_{\rm iso}^{3,4}(\nu)=D_3(\nu)+2D_4(\nu)$, $D_{\rm aniso}^{3,4}(\nu)=D_3(\nu)-D_4(\nu)$. The four composite line shapes were fitted using an appropriate basis set consisting of three moments $\mathbf{a}_0^{(2)}(\|)$, $\mathbf{a}_0^{(2)}(\perp)$, and $\mathbf{a}_{2+}^{(2)}(\perp)$ for each of the four geometries (i.e., nine basis line shapes in total). For fitting we used nonlinear least-squares minimization employing both simulated annealing and Levenberg–Marquardt methods.[30] We found that it was not necessary to include the $\mathbf{a}_{1+}^{(2)}(\|,\perp)$ parameter to get a very good fit to the data, therefore, $\mathbf{a}_{1+}^{(2)}(\|,\perp)=0$ within uncertainties. We found that omitting any of the three fitted parameters led to a very poor fit. Fitted composite anisotropic line shapes are shown in Fig. 10. The fitted parameters $\mathbf{a}_q^{(2)}(p)$ are tabulated in Table III, along with their J-dependent limiting values.

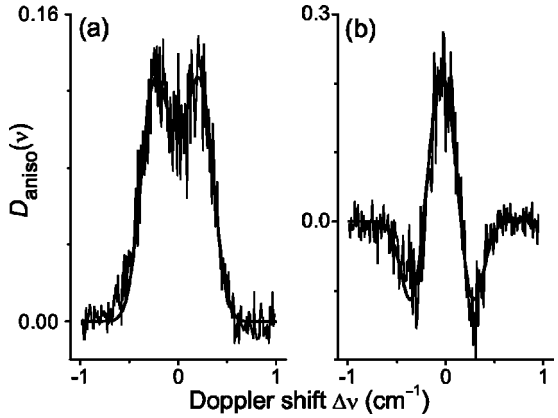

FIG. 10. $P_1(5)$ composite anisotropic doppler line shapes (thin solid lines) and corresponding fits (thick solid lines). The data were taken at the photolysis wavelength 355 nm. (a) $D_{\rm aniso}^{1,2}(\nu)$, (b) $D_{\rm aniso}^{3,4}(\nu)$. The ordinate scales shown are relative to the respective $D_{\rm iso}(\nu)$, normalized to unit area. Note that (b) has a visibly large contribution from β, but contains significant polarization information.

The results in Table III clearly show two important molecule frame alignment effects. The first effect is alignment along the velocity (i.e., the molecule frame z axis), represented by the positive $\mathbf{a}_0^{(2)}(\|)$ and $\mathbf{a}_0^{(2)}(\perp)$ moments. The second effect is alignment along the x axis, indicated by the positive $\mathbf{a}_{2+}^{(2)}(\perp)$. The alignment of $\boldsymbol{J}$ along $\boldsymbol{v}$ can be ascribed to torsion of the OH bond around the O–O axis.[5–11] When the molecule is excited to the $\tilde{A}$ and $\tilde{B}$ states, the OH fragments will twist towards either the trans $\tilde{A}$ conformation ($\phi_d=180°$), or the cis $\tilde{B}$ conformation ($\phi_d=0°$), resulting in the observed alignment of $\boldsymbol{J}$ along $\boldsymbol{v}$. The potential wells for the excited states are much steeper compared with the ground $\tilde{X}$ state, and so the generated torque will be sizeable.[29] Comparison of the relative magnitudes of the $\mathbf{a}_0^{(2)}(p)$ moments shows that $\mathbf{a}_0^{(2)}(\|)$ is slightly larger than $\mathbf{a}_0^{(2)}(\perp)$. This greater degree of alignment from the $\tilde{B}$ state implies a greater torque, and is in qualitative agreement with quantum mechanical simulations by Zhang and co-workers.[31]

TABLE III. Molecule frame alignment and orientation moments determined from Doppler line shapes for the $P_1(5)$ and ${}^{P}Q_{12}(1)$ transitions. Note that the absolute sign of the $\mathbf{a}_q^{(1)}(\|,\perp)$ were not determined; see text for details.

Transition	Parameter	Experimental value	Limits
$P_1(5)$	$\mathbf{a}_0^{(1)}$	0.077 ± 0.020	$-0.920\cdots+0.920$
	$\mathbf{a}_0^{(2)}(\|)$	0.45 ± 0.27	$-1.000\cdots+1.538$
	$\mathbf{a}_0^{(2)}(\perp)$	0.34 ± 0.20	$-1.000\cdots+1.538$
	$\mathbf{a}_{2+}^{(2)}(\perp)$	0.18 ± 0.08	$-1.487\cdots+1.487$
${}^{P}Q_{12}(1)$	$\mathbf{a}_0^{(1)}$	-0.046 ± 0.019	$-0.577\cdots+0.577$
	$\mathbf{a}_{1+}^{(1)}$	0.075 ± 0.032	$-0.577\cdots+0.577$

The observed alignment of $\boldsymbol{J}$ along the molecule x axis for molecules excited to the $\tilde{A}$ state can be explained by the symmetric $\nu_2 = 1394\ \mathrm{cm}^{-1}$ and antisymmetric $\nu_6 = 1265\ \mathrm{cm}^{-1}$ bending modes of H–OO–H.[32] The bending modes result in rotation of the OH fragments with J perpendicular both to $\boldsymbol{v}$ and to the breaking O–O bond axis. *Ab initio* calculations show that the H–OO–H bending potential for the $\tilde{A}$ state in the Franck–Condon region is much flatter than the $\tilde{X}$ state, with a minimum that is vertically above the minimum of the $\tilde{X}$ state,[29,33] and so bending energy in the ν_2, ν_6 co-ordinates is effectively channelled into rotation as the molecule dissociates. The $\mathbf{a}_{2+}^{(2)}(\perp)$ represents a preferential alignment along the x axis compared with y, and the projection of the bending angular momentum onto the x and y axes depends on ϕ_d

$$\mathbf{a}_{2+}^{(2)}(\perp) = \sqrt{3}\left\langle \left(\frac{J_x}{J}\right)^2 - \left(\frac{J_y}{J}\right)^2 \right\rangle = -\sqrt{3}\langle \cos\phi_d \rangle, \tag{8}$$

where we have treated $\boldsymbol{J}$ classically. This means that for large $\phi_d > 90°$, $\boldsymbol{J}$ will be aligned preferentially along the molecule x axis. With $\mathbf{a}_{2+}^{(2)}(\perp) = 0.18 \pm 0.08$, we find that $\langle \phi_d \rangle = 96° \pm 2.6°$, which is lower than the ground-state equilibrium value $\phi_d = 112°$. To satisfy energy requirements, Brouard *et al.* noted that the dissociation of H_2O_2 at longer wavelengths must either involve thermally populated vibrational levels of the $\tilde{X}$ state, or preferential excitation of molecules far from equilibrium geometries.[13] Since they did not observe significant differences in their experiments on cooling by gaseous expansion with Ar or He, they tended to prefer the latter explanation.[8,13] Indeed, the average available thermal energy $kT = 204\ \mathrm{cm}^{-1}$ at 293 K is much smaller than the fundamental vibrational frequencies of H_2O_2, with the exception of the lowest-lying torsional state ($\nu_4 = 254\ \mathrm{cm}^{-1}$).[34] Brouard *et al.* proposed that the mean torsional angle $\langle \phi_d \rangle$ of $\tilde{X}$ state molecules that absorb radiation would *decrease* at longer photolysis wavelengths as these molecules are increasingly displaced from the equilibrium $\phi_d = 112°$.[13] Our experimental estimate of a decreased mean torsional angle $\langle \phi_d \rangle = 96°$ shows remarkable evidence in support of this mechanism.

B. Orientation

Molecule frame orientation parameters were determined using geometries 5 and 5′, by scanning over individual Doppler line shapes. Isotropic and anisotropic composite line shapes were calculated $D_{\mathrm{iso}}^{5,5'}(\nu) = D_5(\nu) + D_{5'}(\nu)$, $D_{\mathrm{aniso}}^{5,5'}(\nu) = D_5(\nu) - D_{5'}(\nu)$. Basis line shapes were simulated using Eqs. (2) and (3), and these basis line shapes were used to fit the experimental composite Doppler line shapes. The β values obtained in Sec. V A were multiplied by $-1/2$ to account for the circular polarization of the photolysis laser. Raw data and fits for the $P_1(5)$ and ${}^{P}Q_{12}(1)$ anisotropic line shapes are shown in Fig. 11, and the resulting $\mathbf{a}_0^{(1)}(\perp)$ and $\mathbf{a}_{1+}^{(1)}(\parallel,\perp)$ parameters are given in Table III. Note that the absolute sign of the $\mathbf{a}_q^{(1)}(\parallel,\perp)$ were not determined, although the sign of $\mathbf{a}_{1+}^{(1)}(\parallel,\perp)$ *relative* to $\mathbf{a}_0^{(1)}(\perp)$ was determined in the case of OH($J = 0.5$).

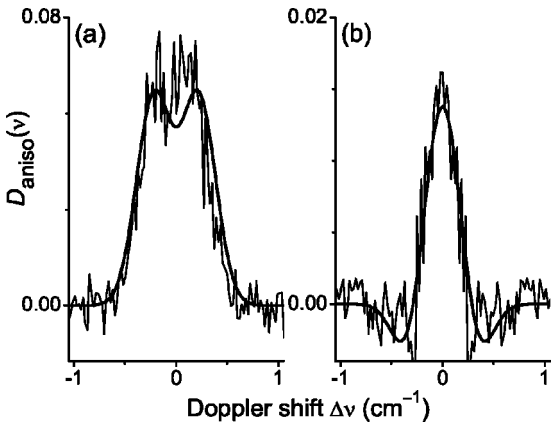

FIG. 11. Composite anisotropic Doppler line shapes $D_{\mathrm{aniso}}^{5,5'}(\nu)$. Results in (a) are for OH($J = 5.5$) $P_1(5)$, the results in (b) are for OH($J = 0.5$) ${}^{P}Q_{12}(1)$. The ordinate scales shown are relative to the respective $D_{\mathrm{iso}}(\nu)$, normalized to unit area.

The $P_1(5)$ results indicate a small orientation $\mathbf{a}_0^{(1)}(\perp)$ in the molecule frame, and we find $\mathbf{a}_{1+}^{(1)}(\parallel,\perp) = 0$ within the limits of our signal to noise. In terms of the electronic coherence between parallel and perpendicular states, the $\mathbf{a}_{1+}^{(1)}(\parallel,\perp)$ parameter contains phase and amplitude information

$$\mathbf{a}_{1+}^{(1)}(\parallel,\perp) \propto N(\parallel,\perp)\cos(\Delta\varphi). \tag{9}$$

In Eq. (9), $\cos(\Delta\varphi) = \cos(\varphi_\perp - \varphi_\parallel)$ is the cosine of the asymptotic phase difference between the radial parts of the outgoing wave functions from parallel and perpendicular transitions. $N(\parallel,\perp)$ represents the relative mixture of parallel and perpendicular states, where $N(\parallel,\perp) = \sqrt{(1+\beta)(1-\beta/2)}$ for photolysis by linearly polarized light, or $N(\parallel,\perp) = \sqrt{(1-2\beta)(1+\beta)}$ for photolysis by circularly polarized light. Note that $\mathbf{a}_{1+}^{(1)}(\parallel,\perp)$ is maximal when there is an equal mixture of parallel and perpendicular states, and the asymptotic phase difference $\Delta\varphi = 0$. The coherent alignment parameter $\mathbf{a}_{1+}^{(2)}(\parallel,\perp)$ also varies with $\cos\Delta\varphi$, and finding $\mathbf{a}_{1+}^{(1)}(\parallel,\perp) = 0$ for $P_1(5)$ is consistent with our finding that $\mathbf{a}_{1+}^{(2)}(\parallel,\perp) = 0$, above.

Comparing the directional properties of $\mathbf{a}_{1+}^{(1)}(\parallel,\perp)$ and $\mathbf{a}_{2+}^{(2)}(\perp)$, we see that the OH($J = 5.5$) are *aligned* but not *oriented* along x. In Sec. V A, we suggested that the $\mathbf{a}_{2+}^{(2)}(\perp)$ resulted from ν_2 and ν_6 bending of the H_2O_2 parent molecule. At any given time, there will be as many OH bonds bending clockwise or anti-clockwise, and it seems reasonable that the circularly polarized photolysis photon has no selectivity upon the phase of this bending motion. Following from the discussion of electronic alignment in Sec. IV C, we suggest that the circular polarization of the photolysis photon causes *electronic* helicity in the molecule frame. The $\mathbf{a}_0^{(1)}(\perp)$ can be written[35]

$$\mathbf{a}_0^{(1)}(\perp) = \frac{m_J}{\sqrt{J(J+1)}}, \tag{10}$$

where m_J is the projection of $\boldsymbol{J}$ onto the z axis ($\boldsymbol{v}$). If we assume that the projection ($1\hbar$) of the angular momentum of the circularly polarized photon on the breaking O–O bond is

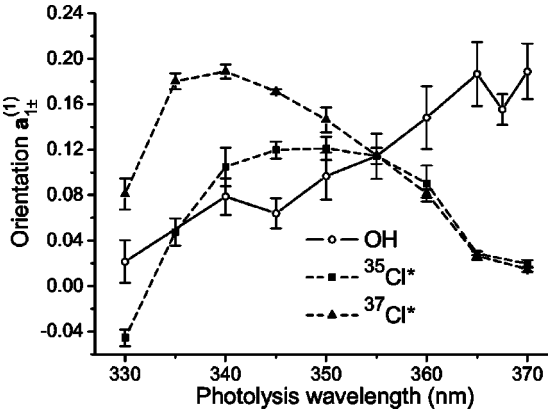

FIG. 12. Dependence of orientation parameter on photolysis wavelength. Solid line: $\mathbf{a}_{1+}^{(1)}(\parallel,\perp)$ for OH($^2\Pi_{1/2}$, $J=0.5$) from dissociation of H_2O_2. Dashed lines: $\mathbf{a}_{1-}^{(1)}(\parallel,\perp)$ for Cl*($^2P_{1/2}$) following dissociation of Cl_2 (Ref. 36). Solid squares are results for ^{35}Cl*, solid triangles for ^{37}Cl*. Note that the OH and Cl* results are real and imaginary parts of $\mathbf{a}_1^{(1)}(\parallel,\perp)$, respectively; see text for details. The H_2O_2 results have been scaled to the ^{37}Cl* at 370 nm by multiplying by 1.52. The overlap of points at 355 nm is coincidental. Note that the absolute sign of $\mathbf{a}_{1+}^{(1)}(\parallel,\perp)$ for OH was not determined.

shared equally between two OH molecules, for OH ($J=5.5$) we find $\mathbf{a}_0^{(1)}(\perp)=0.084$, which is very close to the experimental value $\mathbf{a}_0^{(1)}(\perp)=0.077$ that we measure.

In Sec. IV B we showed that laboratory alignment $\langle A_0^{(2)}\rangle$ of $J=1.5$ molecules was substantially different for OH($^2\Pi_{3/2}$) compared with OH($^2\Pi_{1/2}$) molecules. Significantly, these molecules differ in the amount of rotational versus electronic angular momentum. Molecule frame orientation parameters for $^PQ_{12}(1)$, given in Table III show both an incoherent $\mathbf{a}_0^{(1)}(\perp)$, and a coherent $\mathbf{a}_{1+}^{(1)}(\parallel,\perp)$. Similarly to the OH($^2\Pi_{3/2}$, $J=1.5$), the angular momentum of the OH ($^2\Pi_{1/2}$, $J=0.5$) molecules is purely electronic. Since $\mathbf{a}_{1+}^{(1)}(\parallel,\perp)$ and $\mathbf{a}_{1+}^{(2)}(\parallel,\perp)$ parameter both vary with $\cos(\Delta\varphi)$, it is very likely that interference between the $\tilde{A}(\perp)$ and $\tilde{B}(\parallel)$ states is responsible for both the anomalous alignment of F_1 ($J=1.5$) molecules and the coherent orientation of F_2 ($J=0.5$).

An important aspect of the relationship between $\mathbf{a}_{1+}^{(1)}(\parallel,\perp)$ and $\cos(\Delta\varphi)$ in Eq. (9) is that $\Delta\varphi$ depends implicitly on the total energy available to the photofragment, and the potential energy landscapes $V(\boldsymbol{R})$ encountered for molecules dissociating via parallel and perpendicular states, where $\boldsymbol{R}$ represents the set of nuclear coordinates.[36] To test this dependence, we made measurements of $\mathbf{a}_{1+}^{(1)}(\parallel,\perp)$ in the wavelength region 330–370 nm. Due to constraints of our laser system we were unable to make measurements at wavelengths longer than 370 nm. The results are shown in Fig. 12, along with results from photolysis of Cl_2 across the same wavelength region.[36] Kim *et al.* photolyzed Cl_2 using linearly polarized light, and detected the Cl*($^2P_{1/2}$) product atoms using circularly polarized light. The orientation parameter that they measured was imaginary $\mathrm{Im}[\mathbf{a}_1^{(1)}(\parallel,\perp)] = -\sqrt{2}\mathbf{a}_{1-}^{(1)}(\parallel,\perp)$. The results for H_2O_2 in the present work are real, where $\mathrm{Re}[\mathbf{a}_1^{(1)}(\parallel,\perp)]=-\sqrt{2}\mathbf{a}_{1+}^{(1)}(\parallel,\perp)$. The $\mathbf{a}_{1-}^{(1)}(\parallel,\perp)$ parameter depends on the sine of the asymptotic phase difference

$$\mathbf{a}_{1-}^{(1)}(\parallel,\perp)\propto N(\parallel,\perp)\sin(\Delta\varphi). \tag{11}$$

For a given parent molecule and photofragment, oscillations in $\mathbf{a}_{1-}^{(1)}(\parallel,\perp)$ will be shifted in photolysis energy relative to the $\mathbf{a}_{1+}^{(1)}(\parallel,\perp)$ as a consequence of the 90° phase between $\cos(\Delta\varphi)$ and $\sin(\Delta\varphi)$. Put simply, the interference would be minimum for $\mathbf{a}_{1-}^{(1)}(\parallel,\perp)$ when it was a maximum for $\mathbf{a}_{1+}^{(1)}(\parallel,\perp)$. In the present case, we compare the photolysis of two different systems, and yet the $\mathbf{a}_{1\pm}^{(1)}(\parallel,\perp)$ qualitatively appear to be $\sim 90°$ out of phase.

For H_2O_2 dissociation with linearly polarized light Brouard *et al.* found that $\beta=-0.76\pm0.19$ at 308 nm, and $\beta=+0.83\pm0.19$ at 390 nm, indicating that the transition moves from being 92% perpendicular at 308 nm to being 39% perpendicular at 390 nm.[13] The $\mathbf{a}_{1+}^{(1)}(\parallel,\perp)$ results for OH($J=0.5$) are consistent with the measurements of β: The interference drops to near zero at short wavelengths (320 nm) where the transition is nearly pure perpendicular, and rises to a maximum at longer wavelengths where the transition is mixed. At much longer wavelengths 440–465 nm, Brouard *et al.* found that $\beta=1.7\pm0.2$. In the 440–465 nm region, the dissociation becomes very close to the energetic threshold for dissociation, and we would expect oscillations in $\cos(\Delta\varphi)$ to be more frequent as the total available energy becomes comparable to the difference in potential energy between $\parallel$ and $\perp$ dissociating states.[37] Therefore, the measurement of $\mathbf{a}_{1+}^{(1)}(\parallel,\perp)$ at wavelengths >370 nm would be very interesting for a future study.

That we measure interference for the H_2O_2 photodissociation is, perhaps, remarkable in itself. The Cl* atom results of Kim *et al.*, and previous measurements of coherence in atomic polarization, were all carried out on cooled gaseous expansions.[2,36] The present results were obtained from a flowing room temperature sample. One would expect that the increased number of degrees of freedom for the potential energy surface, and thermal averaging over the initial configurations of the molecule would lead to a blurring of the phase, and a decreased $\mathbf{a}_{1+}^{(1)}(\parallel,\perp)$. However, the energy requirements of the dissociation around 355 nm, supported by the alignment results presented here, do suggest that a very selective subset of ground state H_2O_2 molecules are excited and go on to dissociate. It seems plausible that this selection process would narrow the dissociating wave packet produced on the excited states, leading to the observed interference.

VI. CONCLUSIONS

Angular momentum polarization of OH($^2\Pi$) products following photodissociation of H_2O_2 near 355 nm has been studied in detail. Rotational distributions, spin–orbit branching ratios and lambda-doublet population ratios have been presented. The fraction of available energy going into rotation was small: peaking at $N\approx3$, $\langle f_{\mathrm{rot}}\rangle=4.5\%$, with no preference for either spin–orbit state. Lambda-doublet formation showed that $\Pi(A')$ was more populated than $\Pi(A'')$ at $N=3$.

Integrated laboratory alignment for OH products was small $\langle A_0^{(2)}\rangle<0.15$, and was roughly independent of J, except for OH($^2\Pi_{3/2}$) at $J=1.5$ where electronic alignment

was found to dominate over rotational alignment. The symmetry of the H_2O_2 molecule is pseudo-diatomic, and simple expressions were derived for the angular momentum polarization in the molecule frame. Molecule frame alignment $\mathbf{a}_0^{(2)}(\|)=0.45\pm0.27$, $\mathbf{a}_0^{(2)}(\perp)=0.34\pm0.20$ for OH($^2\Pi_{3/2}$, $J=5.5$) indicated strong alignment of $\boldsymbol{J}$ along $\boldsymbol{v}$ for transitions to both the $\tilde{A}(\perp)$ and $\tilde{B}(\|)$ states, resulting from change in torsional conformation on accessing the excited states. The alignment of OH was found to be noncylindrically symmetric about $\boldsymbol{v}$, and this was related to the mean dihedral angle between the OH bonds in the H_2O_2 molecule $\langle\phi_d\rangle=96°$, which is less than the equilibrium value $\phi_d=112°$ of the ground state. The low experimental estimate of $\langle\phi_d\rangle$ supports the theory of Brouard *et al.* that nonequilibrium ground state H_2O_2 molecules are dissociated.[13]

Molecule frame orientation of OH($\Pi_{3/2}$, $J=5.5$) was found to be $\mathbf{a}_0^{(1)}(\perp)=0.077\pm0.020$, which we believe to be due to electronic orientation. Orientation of OH($\Pi_{1/2}$, $J=0.5$) was found to be $\mathbf{a}_0^{(1)}(\perp)=-0.046\pm0.019$ and $\mathbf{a}_{1+}^{(1)}(\|,\perp)=0.075\pm0.032$. The $\mathbf{a}_{1+}^{(1)}(\|,\perp)$ represents electronic orientation due to interference between dissociating states from parallel and perpendicular transitions. Measurements of $\mathbf{a}_{1+}^{(1)}(\|,\perp)$ as a function of photolysis wavelength were directly compared with measurements of $\mathbf{a}_{1-}^{(1)}(\|,\perp)$ for $Cl^*(^2P_{1/2})$ following dissociation of Cl_2 across the same wavelength range. Despite the polyatomic nature of H_2O_2, with increased degrees of freedom, and implicit averaging over room temperature configurations of the parent, the electronic coherence is not washed out. This may be due to enhanced dissociation cross section of a small subset of the ground-state molecules, which are displaced from equilibrium, and therefore, satisfy more restrictive energy requirements at longer photolysis wavelengths.

ACKNOWLEDGMENTS

The author wants to thank Professor John Brown (Oxford, UK), Dr. Mark Brouard (Oxford, UK), Dr. Marcelo de Miranda (Leeds, UK), and Dr. Peter Rakitzis (FORTH IESL, Greece) for useful discussions. I am grateful to Dr. Jorge Luque (SRI, USA) for providing a version of the LIFBASE program that deals with lambda doubling. The loan of a YAG and dye laser system from the UK EPSRC central laser facility loan pool is gratefully acknowledged. Finally, I wish to thank the Royal Society for the award of a University Research Fellowship.

[1] H. Sato, Chem. Rev. **101**, 2687 (2001).
[2] E. R. Wouters, M. Ahmed, D. S. Peterka, A. S. Bracker, A. G. Suits, and O. S. Vasyutinskii, in *Imaging in Chemical Dynamics*, edited by A. G. Suits and R. E. Continetti, ACS Symposium Series, Vol. 770 (American Chemical Society, Washington D.C., 2000). Conversion factors for $\mathbf{a}_q^{(k)}(p)$ in Table III of this reference are taken from Ref. 21, and may not be appropriate at low *J*.
[3] A. J. Alexander and R. N. Zare, Acc. Chem. Res. **33**, 199 (2000).
[4] W. B. DeMore, S. P. Sander, D. M. Golden, R. F. Hampson, M. J. Kurylo, C. J. Howard, A. R. Ravishankara, C. E. Kolb, and M. Molina, JPL Publ. **97-4**, 157 (1997).
[5] A. U. Grunewald, K.-H. Gericke, and F. J. Comes, J. Chem. Phys. **87**, 5709 (1987).
[6] F. J. Comes, K.-H. Gericke, A. U. Grunewald, and S. Klee, Ber. Bunsenges. Phys. Chem. **92**, 273 (1988).
[7] M. P. Docker, A. Hodgson, and J. P. Simons, Faraday Discuss. Chem. Soc. **82**, 25 (1986).
[8] J. August, M. Brouard, M. P. Docker, A. Hodgson, C. J. Milne, and J. P. Simons, Ber. Bunsenges. Phys. Chem. **92**, 264 (1988).
[9] S. Klee, K.-H. Gericke, and F. J. Comes, J. Chem. Phys. **85**, 40 (1986).
[10] K.-H. Gericke, S. Klee, F. J. Comes, J. Chem. Phys. **85**, 4463 (1986).
[11] S. Klee, K.-H. Gericke, and F. J. Comes, Ber. Bunsenges. Phys. Chem. **92**, 429 (1988).
[12] M. D. Likar, J. E. Baggott, A. Sinha, T. M. Ticich, R. L. Vander Wal, and F. F. Crim, J. Chem. Soc., Faraday Trans. 2 **84**, 1483 (1988).
[13] M. Brouard, M. T. Martinez, C. J. Milne, J. P. Simons, and J.-X. Wang, Chem. Phys. Lett. **165**, 423 (1990).
[14] E.-A. Reinsch, Chem. Phys. Lett. **141**, 369 (1987).
[15] A. C. Kummel, G. O. Sitz, and R. N. Zare, J. Chem. Phys. **88**, 7357 (1988). Note that E_0^1 for Case A in Table III of this paper should read $(1/\sqrt{2})\sin 2\beta$.
[16] J. Luque and D. R. Crosley, LIFBASE: Database and Spectral Simulation Program (Version 1.6), SRI International Report MP 99-009 (1999).
[17] L. D. A. Siebbeles, M. Glass-Maujean, O. S. Vasyutinskii, J. A. Beswick, and O. Roncero, J. Chem. Phys. **100**, 3610 (1994).
[18] A. S. Bracker, E. R. Wouters, A. G. Suits, and O. S. Vasyutinskii, J. Chem. Phys. **110**, 6749 (1999).
[19] T. P. Rakitzis and R. N. Zare, J. Chem. Phys. **110**, 3341 (1999).
[20] M. P. de Miranda, F. J. Aoiz, L. Bañares, and V. Sáez Rábanos, J. Chem. Phys. **111**, 5368 (1999). Note that Eq. (A7) of this reference can be used to convert the polarization parameters of Miranda *et al.* to the $A_q^{(k)}$ and $\mathbf{a}_q^{(k)}$ used in the present work.
[21] T. P. Rakitzis, G. E. Hall, M. L. Costen, and R. N. Zare, J. Chem. Phys. **111**, 8751 (1999). Note that this paper deals with the semiclassical formalism of Dixon, and some of the equations may not be appropriate at low *J*.
[22] M. Ahmed, D. S. Peterka, A. S. Bracker, O. S. Vasyutinskii, and A. G. Suits, J. Chem. Phys. **110**, 4115 (1999).
[23] Z. H. Kim, A. J. Alexander, and R. N. Zare, J. Phys. Chem. A **103**, 10144 (1999).
[24] R. N. Dixon, J. Chem. Phys. **85**, 1866 (1986).
[25] B. V. Picheyev, A. G. Smolin, and O. S. Vasyutinskii, J. Phys. Chem. A **101**, 7614 (1997).
[26] T. P. Rakitzis, S. A. Kandel, A. J. Alexander, Z. H. Kim, and R. N. Zare, J. Chem. Phys. **110**, 3351 (1999).
[27] M. D. Likar, J. E. Baggot, A. Sinha, T. M. Ticich, R. L. Vander Wal, and F. F. Crim, J. Chem. Soc., Faraday Trans. 2 **84**, 1483 (1988).
[28] M. H. Alexander and P. J. Dagdigian, J. Chem. Phys. **80**, 4325 (1984).
[29] A. Morita and S. Kato, J. Phys. Chem. **92**, 1067 (1992).
[30] W. H. Press, S. A. Teukolsky, W. T. Vetterling, and B. P. Flannery, *Numerical Recipes in Fortran*, 2nd ed. (Cambridge University Press, Cambridge, 1992).
[31] Z. T. Cai, D. H. Zhang, and J. Z. H. Zhang, J. Chem. Phys. **100**, 5631 (1994).
[32] P. J. Linstrom and W. G. Mallard, editors, NIST Chemistry WebBook, NIST Standard Reference Database Number 69, July 2001, National Institute of Standards and Technology, Gaithersburg, MD 20899 (http://webbook.nist.gov).
[33] K. Takeshita and P. K. Mukherjee, Chem. Phys. **182**, 195 (1994).
[34] J. Koput, S. Carter, and N. C. Handy, J. Phys. Chem. A **102**, 6325 (1998).
[35] R. N. Zare, *Angular Momentum: Understanding Spatial Aspects in Chemistry and Physics* (Wiley, New York, 1988).
[36] Z. H. Kim, A. J. Alexander, S. A. Kandel, T. P. Rakitzis, and R. N. Zare, Faraday Discuss. Chem. Soc. **113**, 27 (1999).
[37] T. P. Rakitzis, S. A. Kandel, A. J. Alexander, Z. H. Kim, and R. N. Zare, Science **281**, 1347 (1998).